

Answers to frequently asked questions about the pulsar timing array Hellings and Downs correlation curve

Joseph D. Romano*

*Department of Physics and Astronomy, Texas Tech University, Box 41051, Lubbock, TX 79409-1051, USA and
Department of Physics and Astronomy, University of Texas Rio Grande Valley,
One West University Boulevard, Brownsville, TX 78520, USA*

Bruce Allen†

*Max Planck Institute for Gravitational Physics (Albert Einstein Institute),
Leibniz Universität Hannover, Callinstrasse 38, D-30167 Hannover, Germany*

(Dated: August 14, 2023)

We answer frequently asked questions (FAQs) about the Hellings and Downs correlation curve—the “smoking-gun” signature that pulsar timing arrays (PTAs) have detected gravitational waves (GWs). Many of these questions arise because of intuition based on how ground-based interferometers like LIGO respond to GWs. These have arms that are short (km scale) compared to the wavelengths of the GWs that they detect (hundreds to thousands of km). In contrast, PTAs respond to GWs whose wavelengths (tens of light-years) are much shorter than their arms (a typical PTA pulsar is thousands of light-years from Earth). To elucidate this, we calculate the exact response of a “one-arm, one-way” detector to a passing GW, and compare it in the “short-arm” (LIGO-like) and “long-arm” (PTA) limits. This provides qualitative and quantitative answers to many questions about the Hellings and Downs correlation. The resulting “FAQ sheet” should help in understanding the “evidence for GWs” recently announced by several PTA collaborations.

I. INTRODUCTION

Four pulsar timing array (PTA) collaborations recently announced the results of their latest searches for correlated low-frequency ($\sim 10^{-9}$ Hz) gravitational waves (GWs). Their findings span the range from “weak evidence” [1] to “some evidence” [2] to “evidence/marginal evidence” [3] to “compelling evidence” [4].

These observations can be challenging to understand, because the “signal” is unlike the short duration (~ 0.25 s) GW “chirp signal” that LIGO observed on 14 Sep 2015, from the final inspiral and merger of two $\sim 30M_{\odot}$ black holes. Instead of such short (1 s) audio-frequency (100 Hz) deterministic GW signals, PTAs search for persistent (years) low-frequency (nHz) stochastic GW signals. These are too feeble to observe directly, but should produce correlated perturbations in the arrival times of pulses from an array of galactic millisecond pulsars.

Although the current PTA observations are not significant enough to allow one to identify the source of the correlated signal, a credible candidate is the superposition of GWs from hundreds of thousands of supermassive ($\sim 10^9 M_{\odot}$) black-hole (SMBH) binaries orbiting one another in the centers of merging galaxies. While any one of those binaries would produce a deterministic almost-constant-frequency signal, the incoherent sum of many such sources creates a stochastic hubub of GWs.

PTAs search for correlations which are predicted to follow the so-called “Hellings and Downs” curve. This correlation curve is named after Ron Hellings and George Downs, who first derived it in 1983 [5]. The idea is that pulsars act as high-quality clocks, producing radio pulses that arrive at Earth with very predictable and regular arrival times. GWs induce slight perturbations in these arrival time, and these perturbations (called “timing residuals”) are correlated between different radio pulsars.

The Hellings and Downs curve is a plot of the expected correlation in the timing residuals from a pair of pulsars, as a function of their angular separation on the sky. It is a prediction of general relativity (GR) for a gravitational-wave background (GWB) that is unpolarized and isotropic. Figure 1 shows how the timing residuals in NANOGrav’s 15-year dataset [4] appear to match this predicted Hellings and Downs curve.

The goal of this paper is to provide qualitative and quantitative answers to common questions about the properties of the Hellings and Downs correlation curve. We believe that such questions frequently arise because much of our intuition regarding the response of a detector to a passing GW was developed for ground-based GW detectors such as LIGO and Virgo. Not all of this intuition carries over to the case of PTAs. This is because the distance between

* joseph.d.romano@gmail.com

† bruce.allen@aei.mpg.de

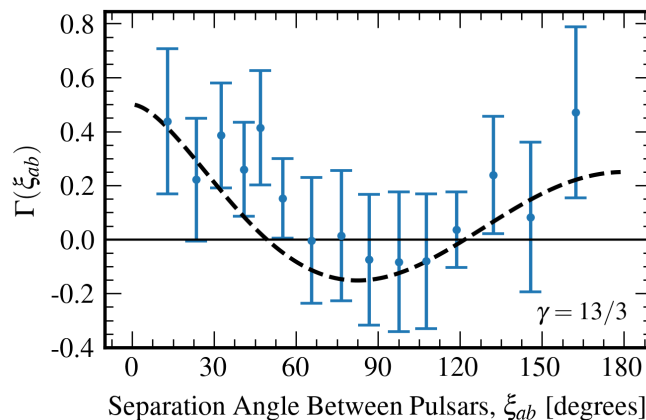


FIG. 1. The spatial correlations observed in the pulsar timing residuals for the NANOGrav 15-year dataset [4] are shown in blue; the Hellings and Downs prediction is shown in black. The blue points and error bars are optimally weighted averages of approximately 150 pulsar-pair correlations in each angular separation bin, which take into account covariances between the correlations induced by the GWB itself. (Figure taken from [4].)

the Earth and a pulsar (one “arm” of a PTA detector) is typically hundreds to thousands of times longer than the wavelengths (tens of light-years) of the GWs that PTAs are trying to detect. In contrast, ground-based interferometers have km-long arms that are much shorter than the wavelengths (100’s to 1000’s of km) of the GWs that these detectors are sensitive to. In short, PTA detectors operate in the “long-arm” (or short-wavelength) limit, whereas ground-based laser interferometers operate in the “short-arm” (or long-wavelength) limit.

The remainder of this paper is organized as follows: We begin immediately with the questions and answers in Section II, developing the formal treatment on an “as needed” basis. The most important concepts are: (i) the exact (timing residual) response of a “one-arm, one-way” detector to a passing GW, and (ii) the expected correlation of two different detectors, expressed in terms of their individual response functions. Limiting expressions for these then give the response and correlation for “short-arm” LIGO-like detectors, and “long-arm” PTA pulsar detectors.

For pedagogical purposes, we also suggest exercises for the reader, but don’t provide solutions. Instead, for the more involved exercises, we point to specific relevant materials in the published literature.

Although the “Hellings-and-Downs correlation FAQ sheet” is the main content of the paper, we conclude with a brief summary in Section III.

II. FREQUENTLY ASKED QUESTIONS

Q1: *Why is the Hellings and Downs correlation normalized at zero angular separation to 1/3 in some papers (e.g., [5 and 6]) and to 1/2 in this FAQ sheet and other papers (e.g., [4 and 7])? Does it matter?*

A1: This normalization difference is an overall scale: multiply the Hellings and Downs curve by a factor of 2/3 to go in one direction, or by 3/2 to go in the other. This choice of normalization is completely arbitrary and makes no difference: any physically observable quantity (for example, the expected time-averaged product of the timing residuals of two pulsars) is independent of this normalization.

The reason why 1/3 and 1/2 have appeared in the literature is historical. The Hellings and Downs correlation was first computed (i) as the *average* product of the timing residual responses of two pulsars to a unit-amplitude GW source, averaged over the sphere of GW source directions. This average introduces a factor of $1/4\pi$ in (2.23). Later, the Hellings and Downs correlation was re-interpreted as (ii) a *correlation coefficient* for the timing residuals of two pulsars, responding to the same GW source. This introduces a factor of $3/8\pi$ in (2.23), which is the normalization choice used in this paper. In case (i) we get 1/3 if the pulsars are distinct but close in sky direction, whereas in case (ii) we get 1/2 if the pulsars are distinct but close on the sky, and 1 (an *auto-correlation*) for two identical pulsars.

Q2: *Why does the Hellings and Downs correlation have different values at 0° and 180° if the quadrupolar deformation of space produced by a passing GW affects two test masses 180° apart in exactly the same way?*

A2: This simple question gets to the heart of the difference between “short-arm” LIGO-like detectors and “long-arm” PTA detectors. Recall that a short-arm detector has $fL/c = L/\lambda \ll 1$, where L is the length of the detector

arm and $\lambda \equiv c/f$ is the GW wavelength. A long-arm detector has $L/\lambda \gg 1$. (Here and throughout, c denotes the speed of light, which is also the propagation speed of GWs.)

A quick, qualitative answer to this question is that for normal incidence of a GW on either a short-arm or long-arm detector, the response of two pulsars in opposite directions will be identical. But for non-normal incidence on a long-arm detector, the response of the two pulsars will be different from one another, because their radio pulses encounter different phases of the GW as they propagate from the pulsars to Earth. Pulses from one of the pulsars will be (partially) “swimming with the current” of the GW as they travel from the pulsar to Earth. In contrast, pulses from the other pulsar will “swim against the current” or “fight upstream” and pass through more cycles of the GW. Since a GWB is composed of GWs coming from many different directions on the sky, the correlated response of two pulsars oriented in opposite directions will differ from that for two pulsars oriented along the same direction. Several illustrative examples are shown in Figure 2.

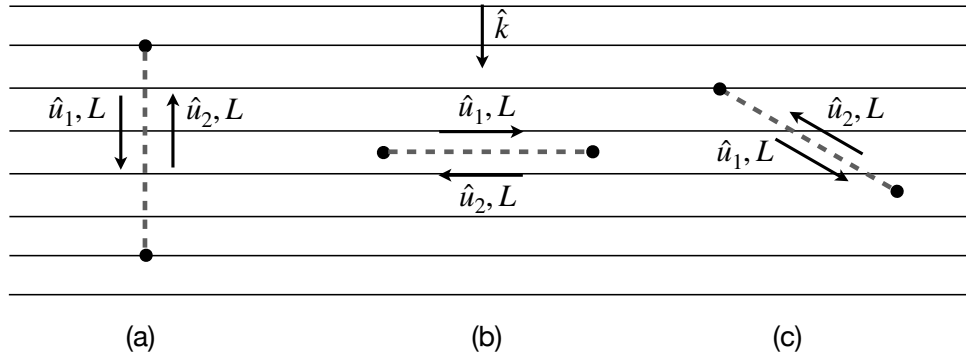


FIG. 2. A monochromatic plane GW propagating in direction \hat{k} passes by six “one-arm, one-way” detectors with arm length L . These have different propagation directions \hat{u} for the electromagnetic waves that monitor the distance between two “test masses” (dots). For PTAs, \hat{u} is the propagation direction of a radio pulse from pulsar to Earth, and $\hat{p} = -\hat{u}$ is the direction to the pulsar on the sky. All six detectors have $L = 5\lambda$; the solid horizontal lines indicate the maxima of the GW at one moment in time. After reading this section, the reader should be able to show that: for case (a), both detectors have zero response to the GW because the radio pulses propagate parallel to the propagation direction of the GW; for case (b), both detectors have zero response to the GW because the radio pulses pass through an integer number of GW cycles during their transit from pulsar to Earth; for case (c) with $\hat{k} \cdot \hat{u}_1 = -\hat{k} \cdot \hat{u}_2 = 1/2$, the radio pulse moving in direction \hat{u}_1 (partially) “surfs” the GW so that this detector has a $3\times$ larger response to the GW than for the detector with pulse direction \hat{u}_2 .

In order to give a more complete and quantitative answer to this question, we need to understand how a generic “one-arm, one-way” detector responds to a passing GW. We will then combine the resulting response functions to obtain the expected correlation, obtaining the Hellings and Downs curve. For presentation purposes, we split the following discussion into a few main parts.

A. Calculating the timing residual response

The geometry of a one-arm detector, where the electromagnetic signal (from a pulsar or laser) travels in just one direction along that arm, is shown in Figure 3. Such “beam detectors” use electromagnetic radiation to monitor the separation of two or more freely-falling masses. Laser interferometers (both ground- and space-based), spacecraft Doppler tracking, and PTAs are all examples of beam detectors.

As a GW passes by the detector, it will “stretch” and “squeeze” space perpendicular to its direction of propagation \hat{k} (see the upper right panel of Figure 4). This quadrupolar deformation of space causes the electromagnetic signal (which we will treat generically here as a photon) to arrive either slightly earlier or later than it would in the absence of a GW. The size of the advance or delay in the photon arrival time will depend on the orientation of the detector (defined by the unit vector \hat{u}) relative to \hat{k} , and the length of the arm L relative to the wavelength of the GW, i.e., L/λ or equivalently fL/c . We will denote this change in the arrival time by $\Delta T(t)$, which is a function of the time t that the observation is made.

An explicit formula for $\Delta T(t)$ involves the metric perturbations $h_{ij}(t, \vec{x})$, which contain all information about the GWs. In fact, $\Delta T(t)$ only depends upon the metric perturbations along the spacetime path followed by the photon

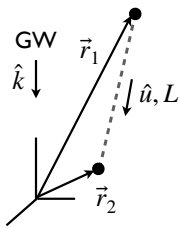


FIG. 3. Geometry of a one-arm, one-way beam detector. The GW propagates in the \hat{k} direction; the electromagnetic wave (e.g., a radio pulse from a pulsar, or laser light traveling between two mirrors) propagates in the \hat{u} direction, opposite the direction from Earth to the pulsar, or from the second test mass to the first test mass, $\hat{p} = -\hat{u}$. Here, L is the “arm” length of the detector.

as it moves through the GW detector, arriving at time t :

$$\Delta T(t) = \frac{1}{2c} u^i u^j \int_0^L ds h_{ij}(\tau(s), \vec{x}(s)). \quad (2.1)$$

From this equation, you can see that the photon moving through the detector is “sampling” the GW field h_{ij} along its spacetime path $(\tau(s), \vec{x}(s))$.

That spacetime path is described by the parametric representation $\tau(s) = t + (s - L)/c$ and $\vec{x}(s) = \vec{r}_1 + s\hat{u}$. The parameter s starts at 0 (photon emission) and increases smoothly to L (photon reception). This spacetime path is a straight line in 4-dimensional spacetime, starting at the point $(t - L/c, \vec{r}_1)$ and ending at the point (t, \vec{r}_2) . The reader should verify that the magnitude of the velocity vector $d\vec{x}/d\tau = (d\vec{x}/ds)(ds/d\tau)$ is the speed of light.

We will use $t_1 \equiv t - L/c$ to denote the time that the photon left the source at \vec{r}_1 , and $t_2 \equiv t$ to be the time that the photon was received at the receiver at $\vec{r}_2 \equiv \vec{r}_1 + L\hat{u}$. Note that we do not need to include any corrections to the straight-line path for the photon given above, as the metric perturbations are already first-order small and we can ignore all second and higher-order terms in the calculation.

To do the integral we need an explicit expression for the metric perturbations. Recall that GWs are time-varying perturbations to the geometry of space-time, which propagate away from the source at the speed of light, see e.g., [8 and 9]. In transverse-traceless coordinates $(t, \vec{x}) \equiv (t, x^i)$, where $i = 1, 2, 3$, the metric perturbations corresponding to a plane wave have two degrees of freedom, corresponding to the amplitudes of the plus (+) and cross (\times) polarizations of the GW (Figure 4).

The metric perturbations for the most general GW field can be written as a superposition of plane waves:

$$h_{ij}(t, \vec{x}) = \int_{-\infty}^{\infty} df \int d\hat{k} \sum_{A=+, \times} h_A(f, \hat{k}) e_{ij}^A(\hat{k}) e^{i2\pi f(t - \hat{k} \cdot \vec{x}/c)}, \quad (2.2)$$

where f denotes the frequency of the component waves, \hat{k} their direction of propagation, and $A = +, \times$ their polarization. Note that this plane wave expansion can represent *any possible pattern* of GWs: it does not have to be from a stochastic background, and might be from a single deterministic source, or any combination of such (deterministic and/or stochastic) sources. We only need the correct functions $h_A(f, \hat{k})$.

There is only one caveat: this equation does not correctly represent the metric perturbations close to a GW source. But that doesn't matter here. The first significant sources of GWs for these detectors are many of orders of magnitude farther way than L , so in the relevant region of spacetime around the detectors there are no sources, and (2.2) holds.

In thinking about (2.2), it is helpful to imagine that the integral over directions \hat{k} is really a discrete sum, with one term for each (distant) GW source. The direction to a particular GW source is given by $\hat{n} \equiv -\hat{k}$. The quantities $e_{ij}^A(\hat{k})$ with $A = +, \times$ are polarization tensors, defined by

$$e_{ij}^+(\hat{k}) \equiv \hat{l}_i \hat{l}_j - \hat{m}_i \hat{m}_j, \quad e_{ij}^\times(\hat{k}) \equiv \hat{l}_i \hat{m}_j + \hat{m}_i \hat{l}_j, \quad (2.3)$$

where \hat{l}, \hat{m} are any two orthogonal unit vectors in the plane orthogonal to \hat{k} . Conventionally, for stochastic background analyses, we take

$$\begin{aligned} \hat{k} &\equiv -\hat{x} \sin \theta \cos \phi - \hat{y} \sin \theta \sin \phi - \hat{z} \cos \theta, \\ \hat{l} &\equiv \hat{x} \sin \phi - \hat{y} \cos \phi, \\ \hat{m} &\equiv -\hat{x} \cos \theta \cos \phi - \hat{y} \cos \theta \sin \phi + \hat{z} \sin \theta. \end{aligned} \quad (2.4)$$

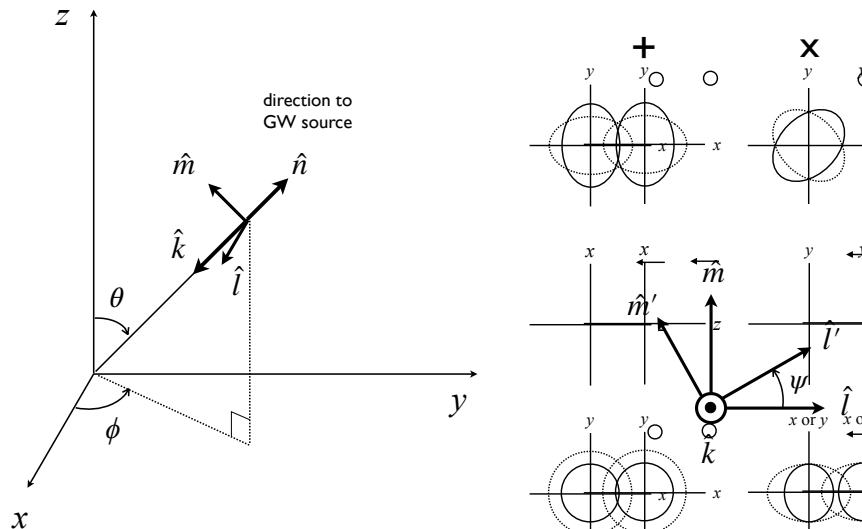


FIG. 4. Left panel: Coordinate system and unit vectors used in the plane wave expansion. Right panel (top): two orthogonal polarizations of a GW. A circular ring of test particles in the plane orthogonal to the propagation direction \hat{k} of the wave are alternately deformed into ellipses, as space is “squeezed” and “stretched” by the passing of the wave. Right panel (bottom): an alternative choice of two orthogonal polarizations may be obtained by rotating \hat{l} and \hat{m} through angle ψ to obtain new vectors \hat{l}' and \hat{m}' .

The reader should verify that these three vectors are *orthonormal*, meaning that each has unit length and is perpendicular to the other two. In fact, $\hat{k} = -\hat{r}$, $\hat{l} = -\hat{\phi}$, $\hat{m} = -\hat{\theta}$, where \hat{r} , $\hat{\theta}$, $\hat{\phi}$ are the standard spherical polar coordinate unit vectors.

For a given GW propagation direction \hat{k} , one can form another (equivalent) orthonormal set by rotating the vectors \hat{l} and \hat{m} by an angle ψ (called the *polarization angle*) in the plane orthogonal to \hat{k} , as shown in the bottom right panel of Figure 4. We leave it as an exercise for the reader to show that such a rotation of \hat{l} and \hat{m} leads to a new set of polarization tensors

$$\begin{bmatrix} e'_{ij}{}^+ \\ e'_{ij}{}^\times \end{bmatrix} = \begin{bmatrix} \cos 2\psi & \sin 2\psi \\ -\sin 2\psi & \cos 2\psi \end{bmatrix} \begin{bmatrix} e_{ij}{}^+ \\ e_{ij}{}^\times \end{bmatrix}. \quad (2.5)$$

This change of polarization basis is a spin-two gauge transformation. It leads to different values of the expansion coefficients $h_A(f, \hat{k})$, but does not change the metric perturbations $h_{ij}(t, \vec{x})$.

Another useful exercise is to define a complex polarization tensor $e_{ij} \equiv e_{ij}^+ - ie_{ij}^\times$, and to show that under (2.5) it transforms to $e'_{ij} = \exp(2i\psi)e_{ij}$. In fact, the “2” that appears in this transformation is the reason why the field is said to have “spin two”. As an alternative to the linear polarization basis, the polarization tensor e_{ij} and its complex conjugate e_{ij}^* form a right- and left-circular polarization basis. (See also Problem 9 from Chapter 16 of [9].)

Returning to (2.1), we first need to substitute $\tau(s)$ and $\vec{x}(s)$ for t and \vec{x} in the plane wave expansion (2.2) for $h_{ij}(t, \vec{x})$. The s dependence shows up only in the exponential, so the integration is easy. Again, we leave it as an exercise for the reader to show that doing the integration and grouping terms accordingly gives

$$\Delta T(t) = \int_{-\infty}^{\infty} df \int d\hat{k} \sum_{A=+, \times} h_A(f, \hat{k}) R^A(f, \hat{k}) e^{i2\pi f(t - \hat{k} \cdot \vec{r}_2/c)}, \quad (2.6)$$

where

$$R^A(f, \hat{k}) \equiv \frac{1}{2} u^i u^j e_{ij}^A(\hat{k}) \frac{1}{i2\pi f} \frac{1}{1 - \hat{k} \cdot \hat{u}} \left[1 - e^{-i2\pi f L(1 - \hat{k} \cdot \hat{u})} \right]. \quad (2.7)$$

(For a solution, see equations (6.8)–(6.10) in [10] or equations (C8)–(C9) in [6] or Appendix B and equations (C1)–(C2) in [7].) The quantity $R^A(f, \hat{k})$ is the *detector response function* for a timing residual measurement made by a one-arm,

one-way detector of length L responding to a plane-polarized GW having polarization A , propagation direction \hat{k} , and frequency f .

Note that we have factored out an exponential term $e^{i2\pi f(t-\hat{k}\cdot\vec{r}_2/c)}$ in the integrand of $\Delta T(t)$. For the case of pulsar timing, the argument of this exponential is the phase of the GW at the time $t \equiv t_2$ and location \vec{r}_2 of the reception of the radio pulse at Earth. It is also easy to show that the product of $e^{i2\pi f(t-\hat{k}\cdot\vec{r}_2/c)}$ and the second term in square brackets in (2.7) is $e^{i2\pi f(t_1-\hat{k}\cdot\vec{r}_1/c)}$. The argument of this exponential is the phase of the GW at the time t_1 and location \vec{r}_1 of the emission of the radio pulse at the pulsar. Hence, in the context of pulsar timing observations, the “1” in square brackets in (2.7) corresponds to the “Earth term” while the exponential in the square brackets corresponds to the “pulsar term”. The direction to the pulsar is $\hat{p} = -\hat{u}$.

The integral leading to (2.7) is the difference between a function evaluated at the upper limit (photon received) and lower limit (photon emitted). The difference has a simple physical explanation first given by Detweiler [11]. Rather than computing the timing residual, he instead gave an (equivalent) analysis in terms of the effect of the GW on the photon’s frequency. In this picture, the GW gives the photon source (pulsar) and photon receiver (Earth) a nonzero velocity. It is the *difference* between these two velocities, projected along the line of sight to the pulsar, which creates (via the Doppler effect) a shift in the photon frequency. If both source and receiver have the same projected velocity, then the Earth and pulsar term cancel, and the GW has no net effect on the photon redshift/pulsar timing residual.

The expression for the timing residual response function (2.7) may be written as a product of two terms: (i) a frequency-independent (but polarization-dependent) geometrical projection factor

$$G^A(\hat{k}) \equiv \frac{1}{2} u^i u^j e_{ij}^A(\hat{k}), \quad (2.8)$$

and (ii) a frequency-dependent (but polarization-independent) *timing transfer function*

$$\mathcal{T}(fL/c, \hat{k} \cdot \hat{u}) \equiv \frac{1}{i2\pi f} \frac{1}{1 - \hat{k} \cdot \hat{u}} \left[1 - e^{-\frac{i2\pi f L}{c}(1 - \hat{k} \cdot \hat{u})} \right]. \quad (2.9)$$

The timing transfer function vanishes when the photon encounters an integer number of complete cycles of GW-induced stretching and squeezing, which integrate to zero net timing delay. At fixed GW frequency f , this occurs for $\text{int}[2fL/c]$ different incident directions, given by values of $\hat{k} \cdot \hat{u}$ that satisfy

$$1 - \hat{k} \cdot \hat{u} = \frac{n}{fL/c} \quad \text{where} \quad n = 1, 2, \dots, \text{int}[2fL/c]. \quad (2.10)$$

The limit on n arises because the lhs of (2.10) lies in the interval $[0, 2]$. However, for a given GW direction (fixed $\hat{k} \cdot \hat{u}$) there are an infinite number of frequencies at which \mathcal{T} vanishes. For normal incidence of the GW on the detector ($\hat{k} \cdot \hat{u} = 0$, as in panel (b) of Figure 2), these zeroes lie at $f = (c/L)n$ for $n = 1, 2, 3, \dots$, as shown in Figure 5.

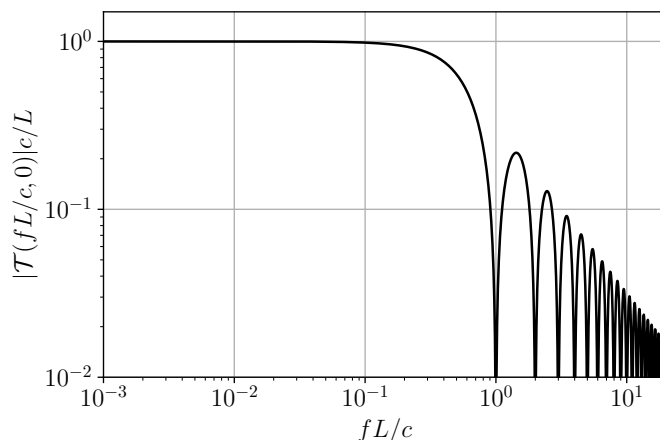


FIG. 5. Modulus of the timing transfer function $\mathcal{T}(fL/c, \hat{k} \cdot \hat{u})$ for a normally incident ($\hat{k} \cdot \hat{u} = 0$) GW. It vanishes when the arm length is a positive integer number of GW wavelengths.

For a short-arm LIGO-like detector, the above expression for the timing transfer function (2.9) and hence the

response function (2.7) simplify considerably. Expanding the exponential in (2.9) to first order in $fL/c \ll 1$ gives

$$\mathcal{T}(fL/c, \hat{k} \cdot \hat{u}) \simeq \frac{L}{c} \quad \Rightarrow \quad R^A(f, \hat{k}) \simeq \frac{1}{2} \frac{L}{c} u^i u^j e_{ij}^A(\hat{k}) \quad (\text{short-arm limit}). \quad (2.11)$$

You can convert this to the more common strain response $h(t) \equiv \Delta L(t)/L$ by simply dividing $\Delta T(t)$ and $R^A(f, \hat{k})$ by the nominal one-way propagation time $T \equiv L/c$ of a photon down the arm of the detector. Then $\mathcal{T} \simeq 1 \Rightarrow R^A(f, \hat{k}) \simeq G^A(\hat{k})$ for the short-arm strain response.

Note that this short-arm response function is symmetric under the interchange $\hat{u} \rightarrow -\hat{u}$. This means that if the distance from the Earth to a pulsar was much less than the GW wavelength, then the timing response of that Earth-pulsar baseline \hat{p} would be exactly the same as that for a pulsar in the opposite sky direction, $-\hat{p}$. This can be seen graphically in the leftmost panels of Figures 6 and 7.

For later use, we define another frequency-independent geometrical projection factor

$$F^A(\hat{k}) \equiv \frac{1}{2} \frac{u^i u^j}{1 - \hat{k} \cdot \hat{u}} e_{ij}^A(\hat{k}), \quad (2.12)$$

which differs from $G^A(\hat{k})$ defined in (2.8) by a factor of $1 - \hat{k} \cdot \hat{u}$ in the denominator. The full timing response function (2.7) may be written as

$$R^A(f, \hat{k}) = \frac{1}{i2\pi f} F^A(\hat{k}) \left[1 - e^{-\frac{i2\pi f L}{c}(1 - \hat{k} \cdot \hat{u})} \right]. \quad (2.13)$$

The extra factor of $1 - \hat{k} \cdot \hat{u}$ comes from the timing transfer function (2.9), and breaks G 's $\hat{u} \rightarrow -\hat{u}$ symmetry. The asymmetry manifests itself graphically in the middle and rightmost panels of Figure 7. The response function $F^A(\hat{k})$ is often called the *Earth-term-only* response function, since it doesn't include the exponential term in square brackets (i.e., the pulsar term) and is thus independent of frequency.

At first glance it appears that $F^A(\hat{k})$ blows up as $\hat{k} \rightarrow \hat{u}$, since the denominator $1 - \hat{k} \cdot \hat{u}$ in (2.12) approaches zero. But this zero in the denominator is cancelled by a zero from the geometrical projection factor $u^i u^j e_{ij}^A(\hat{k})$, so that $F^A(\hat{k} = \hat{u})$ is finite. Actually, the full response function $R^A(f, \hat{k} = \hat{u})$ vanishes, because the two terms in square brackets in (2.13) cancel. This makes sense: a GW deforms space only in the plane *transverse* to its direction of propagation \hat{k} . So when $\hat{k} = \hat{u}$, the radio pulse does not feel these deformations. See Figure 2, panel (a) for an example.

B. Visualizing the timing residual response (antenna pattern functions)

We now work out the timing residual response function of a one-arm, one-way detector to a linearly-polarized GW source at a fixed point in the sky, radiating at a single frequency, and uniformly averaged over linear polarization directions. To compute this, start with a linearly-polarized GW (containing only one of the two possible polarizations (2.3)) and average over the choice of directions \hat{l} and \hat{m} that define what “+” and “×” means. This leads to the *polarization-averaged* response function

$$R(f, \hat{k}) \equiv \left[\frac{1}{2\pi} \int_0^{2\pi} d\psi R^+(f, \hat{k}, \psi) R^{+*}(f, \hat{k}, \psi) \right]^{1/2}. \quad (2.14)$$

Here $R^+(f, \hat{k}, \psi)$ is given by (2.7) with the standard polarization tensors $e_{ij}^+(\hat{k})$ replaced by $e'_{ij}^+(\hat{k}, \psi)$ given in (2.5). (If you are wondering: defining (2.14) with only the × polarization leads to an identical result.)

Since the ψ dependence of the integrand in (2.14) involves quadratic combinations of $\cos 2\psi$ and $\sin 2\psi$, the integral over ψ is an easy exercise for the reader to do, giving

$$R(f, \hat{k}) = \sqrt{\frac{1}{2} \left(|R^+(f, \hat{k})|^2 + |R^\times(f, \hat{k})|^2 \right)} = \frac{1}{\sqrt{2}} G(\hat{k}) |\mathcal{T}(fL/c, \hat{k} \cdot \hat{u})|, \quad (2.15)$$

where

$$G(\hat{k}) \equiv \sqrt{G^+(\hat{k})^2 + G^\times(\hat{k})^2}. \quad (2.16)$$

Such *quadrature combinations* arises whenever we uniformly average over the polarization direction of sources. For the case of a pulsar located in the $\hat{p} = -\hat{u} = \hat{z}$ direction

$$G(\hat{k}) = \frac{1}{2} \sin^2 \theta, \quad F(\hat{k}) = \frac{1}{2} (1 + \cos \theta), \quad (2.17)$$

where $\hat{k} \cdot \hat{u} = \cos \theta$ is the cosine of the angle of the GW relative to the one-arm, one-way detector, and $F(\hat{k})$ is defined by a quadrature combination similar to (2.16). You will need to use (2.3), (2.4), (2.8), and (2.12) to obtain these explicit expressions. Note that, as discussed in the final paragraph of Section II A, F is finite as $\theta \rightarrow 0$ and vanishes as $\theta \rightarrow \pi$ (see the middle panel of Figure 7).

For fixed frequency f and fixed distance L to a pulsar, the *shape* of the polarization-averaged response function $R(f, \hat{k})$ depends only on the relative orientation of the GW propagation direction \hat{k} and the direction to the pulsar $\hat{p} = -\hat{u}$. The shape of $R(f, \hat{k})$ is often called an *antenna pattern*, because the magnitude of R is the “strength” of the response. Figure 6 shows plots of the antenna patterns $R(f, \hat{k})$ for a pulsar located in the \hat{z} direction for different fixed values of fL/c . The left panel shows the antenna pattern in the “short-arm” LIGO-like limit, $fL/c \ll 1$, which is proportional to $\sin^2 \theta$, as shown in (2.11), (2.8), and (2.17). Note that the number of lobes of the antenna pattern increases as fL/c increases, and that the overall magnitude of the antenna pattern function decreases like $1/(2\pi f)$. Both of these behaviors are a consequence of the form of the timing transfer function given in (2.9).

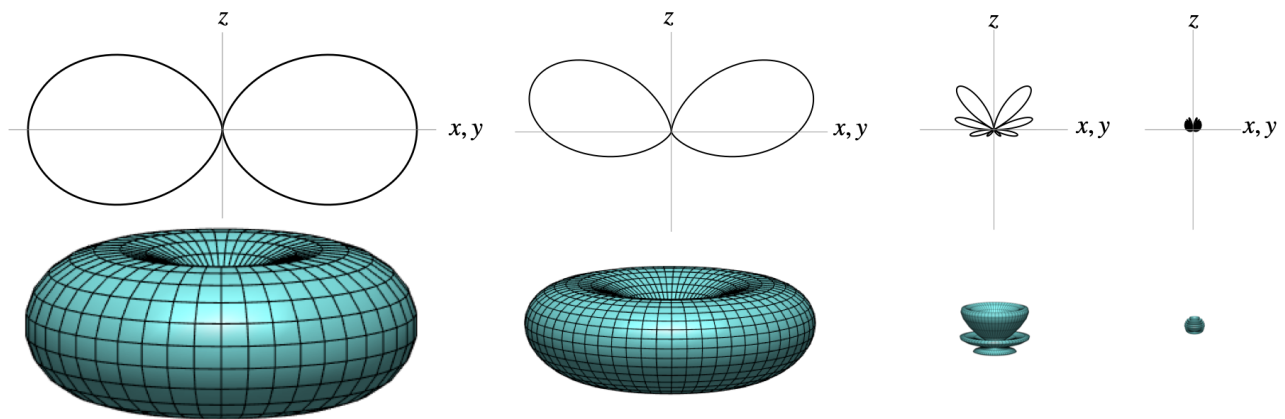


FIG. 6. Antenna pattern functions for the polarization-averaged timing response of a one-arm, one-way detector having $\hat{u} = -\hat{z}$, evaluated for different fixed values of $fL/c = L/\lambda$ (from left to right, $fL/c = 0, 0.5, 2, 10$). The top row of plots are cross-sections: the antenna pattern functions are axially symmetric about the vertical z -axis. For example, the leftmost pattern resembles a donut with no hole, as shown in the bottom row of plots, which are the corresponding antenna patterns viewed from slightly above the xy plane.

Recall that for most pulsars, fL/c will be of order 100 or more, since the distance to typical pulsars is of order a kpc (so a few thousand light-years) or more, while the GW wavelength is only of order tens of light-years. The rightmost panel of Figure 7 shows a rescaled version of $R(f, \hat{k})$ appropriate for the (semi-realistic) case $fL/c = 100$. Also plotted in this figure are the polarization-averaged antenna pattern functions for the geometrical projection factors $G(\hat{k})$ (left panel) and $F(\hat{k})$ (middle panel). Note that $F(\hat{k})$ is half of the “envelope” of the full response function $R(f, \hat{k})$, illustrated by the dashed-white curve in the rightmost panel plot.

C. Calculating overlap functions and the Hellings and Downs correlation

Large amplitude GWs would be directly visible in GW detector output. For example, in the early days of pulsar timing, limits were set on the amplitude of GWs in this way, by examining the timing residuals from single pulsars. But the GWs predicted for typical background sources are too weak to allow this: they cannot be separated from noise in the measurements or other physical effects. Fortunately, there is a way around this: look for a *common* GW signal by correlating the outputs of *two or more* detectors. With sufficient integration or averaging, this allows one to “dig below the noise”.

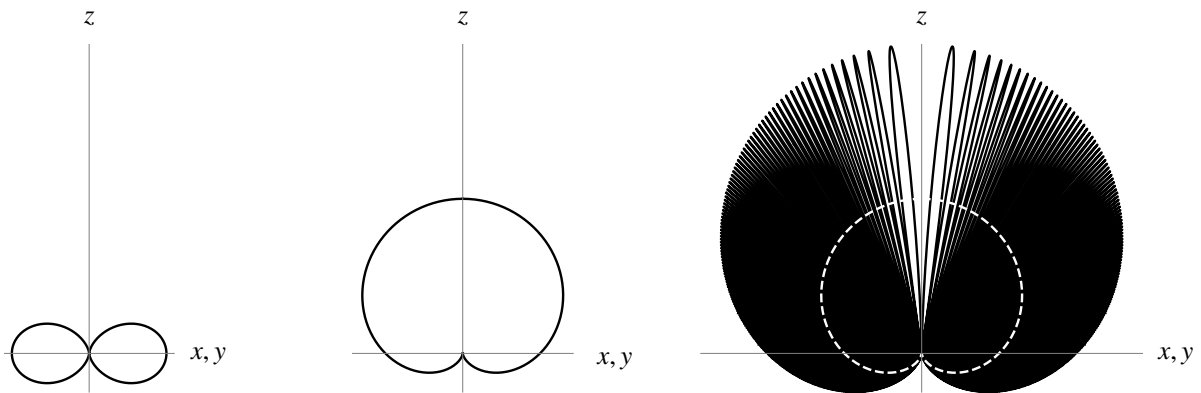


FIG. 7. Antenna pattern functions for the polarization-averaged geometrical projection factors $G(\hat{k})$ (left panel) and $F(\hat{k})$ (middle panel). The right panel compares $F(\hat{k})$ (white dashed curve) with the full polarization-averaged timing response function $R(f, \hat{k})$ for $fL/c = 100$ rescaled by a factor of $2\pi f$ so that it has the same scale as $F(\hat{k})$. All of these antenna pattern functions are axially symmetric around the vertical z -axis.

For this reason, we define the *overlap function* for a pair of detectors, which is proportional to the expected correlation of their outputs. As we shall show below, the Hellings and Downs correlation is an example of an overlap function, calculated in the context of pulsar timing array observations, evaluated for many different pairs of pulsars.

In our Universe, the GW background is (to very high precision) defined by (2.2) for *specific functions* $h_+(f, \hat{k})$ and $h_\times(f, \hat{k})$, which are the Fourier coefficients in the plane wave expansion of the metric perturbations. Sadly, we do not know what these functions are. So, to understand what one might see, and how to interpret the data, we are forced to build imaginary mathematical “model universes”, and ask what might be observed in those. Typically, these model universes assume that the sources have particular distances, sky locations, and so on. But, since we don’t know these values, we have to resort to a statistical approach. We construct many model universes in which these unknowns take on different values, and then ask, “what would we typically observe?” In short, our lack of knowledge about the sources forces us to follow a statistical approach.

The set of model universes is called an “ensemble”. Our Universe itself is *not* an ensemble, although, if we have done a very good job in constructing an ensemble, our Universe might correspond very closely to one of the models in that ensemble. The different models in the ensemble are called “realizations”; each one corresponds to a different specific choice of the functions $h_A(f, \hat{k})$. For example, several different ensembles are explicitly constructed in Section III of [6].

To calculate the expected correlation of a pair of measurements containing stochastic signals, we need to define the ensemble of possible realizations associated with that stochastic process. Expectation values $\langle \rangle$ are averages over the realizations within the ensemble.

For GWB searches, it is common to consider a *Gaussian* ensemble. This is a good choice, because the *central limit theorem* shows that the incoherent sum of many weak processes is well described by such an ensemble.

Since the quantities of interest depend upon $h_{ij}(t, \vec{x})$, which in turn are determined by the Fourier coefficients $h_A(f, \hat{k})$, it is sufficient if we know how to calculate the expected value of products containing any number of these, for example $\langle h_+(f_1, \hat{k}_1)h_+(f_2, \hat{k}_2)h_+(f_3, \hat{k}_3) \rangle$.

A beautiful feature of the Gaussian ensemble was proved more than a century ago [12]: all moments, of any order, are expressible in terms of sums of products of the first two moments, $\langle h_A(f_1, \hat{k}_1) \rangle$ and $\langle h_A(f_1, \hat{k}_1)h_{A'}(f_2, \hat{k}_2) \rangle$. We will assume that these first two moments have the following simple form

$$\langle h_A(f, \hat{k}) \rangle = 0 \quad \text{and} \quad \langle h_A(f, \hat{k})h_{A'}^*(f', \hat{k}') \rangle = \frac{1}{8\pi}H(f)\delta(f - f')\delta_{AA'}\delta^2(\hat{k}, \hat{k}'), \quad (2.18)$$

where the non-negative real function $H(f) = H(-f)$ is the (two-sided) *strain power spectral density* of the background, having units of $\text{strain}^2 \text{Hz}^{-1}$. The first moment is zero since for every realization in the ensemble there is another identical one with its phase shifted by an arbitrary amount. The $\delta(f - f')$ on the rhs of the second moment arises because the ensemble is *stationarity*: there is no preferred origin of time because for every realization in the ensemble, there is another identical one shifted forwards or backwards in time. The $\delta_{AA'}$ implies that the ensemble is *unpolarized*: for every realization, there is another one that is identical except that the \hat{l}, \hat{m} vectors are rotated through an arbitrary

angle ψ . Finally, the factor of $\delta^2(\hat{k}, \hat{k}')$ arises because the ensemble is *spatially homogeneous and isotropic*: for every realization in the ensemble and for every point in space, there is another realization that is related to the first by a rotation about that point by an arbitrary set of Euler angles.

We are now ready to calculate the expected value of two timing residual measurements $\Delta T_a(t)$ and $\Delta T_b(t')$, where the two times t and t' may be different. The indices a and b label the two pulsars; \hat{p}_a and \hat{p}_b will denote their directions on the sky, and L_a and L_b will denote their distances from Earth. We leave it as another exercise for the reader to show that by using (2.18) and (2.6),

$$\langle \Delta T_a(t) \Delta T_b(t') \rangle = \int_{-\infty}^{\infty} df e^{i2\pi f(t-t')} \Gamma_{ab}(f) H(f), \quad (2.19)$$

where

$$\Gamma_{ab}(f) \equiv \frac{1}{8\pi} \int d\hat{k} \sum_A R_a^A(f, \hat{k}) R_b^{A*}(f, \hat{k}) e^{-i2\pi f \hat{k} \cdot (\vec{r}_a - \vec{r}_b)/c} \quad (2.20)$$

is the *overlap function* for the two detectors. The concept of an overlap function is a general construction; it is not restricted to timing residual measurements for pulsar timing arrays, see e.g., [13–15]. From (2.19), one sees that $\Gamma_{ab}(f)$ plays the role of a transfer function relating the expected correlation in the output of two detectors to the auto-correlated power.

To proceed further, we use (2.13) to expand the timing residual response functions in (2.20). This yields

$$\Gamma_{ab}(f) = \frac{1}{(2\pi f)^2} \frac{1}{8\pi} \int d\hat{k} \sum_A F_a^A(\hat{k}) F_b^A(\hat{k}) e^{-i2\pi f \hat{k} \cdot (\vec{r}_a - \vec{r}_b)/c} \times \left[1 - e^{-\frac{i2\pi f L_a}{c} (1 + \hat{k} \cdot \hat{p}_a)} \right] \left[1 - e^{+\frac{i2\pi f L_b}{c} (1 + \hat{k} \cdot \hat{p}_b)} \right], \quad (2.21)$$

where $\hat{p}_a = -\hat{u}_a$ and $\hat{p}_b = -\hat{u}_b$, and where we have crossed off several terms for the following reasons: (i) The argument of the exponential involving the detector locations \vec{r}_a and \vec{r}_b is approximately zero since the separation between two radio telescopes on Earth is much smaller than the wavelength c/f of the GWs that pulsar timing arrays are sensitive to. (In fact the observations are generally referred back to the solar system barycenter (SSB) in which case $\vec{r}_a = \vec{r}_b$.) (ii) For distinct pulsars ($a \neq b$), we can ignore the pulsar terms in the square brackets, since the two Earth-pulsar product terms and the single pulsar-pulsar product term are rapidly varying function of \hat{k} and do not contribute significantly when integrated over the whole sky, see [5] and [7]. However, for the auto-correlation of a single pulsar with itself (i.e., $a = b$), the product of the two pulsar terms equals 1 and hence cannot be ignored. Thus,

$$\Gamma_{ab}(f) = \frac{1}{(2\pi f)^2} \frac{1}{8\pi} \int d\hat{k} \sum_A F_a^A(\hat{k}) F_b^A(\hat{k}) [1 + \delta_{ab}] = \frac{1}{12\pi^2 f^2} \Gamma_{ab}, \quad (2.22)$$

where

$$\Gamma_{ab} \equiv \frac{3}{8\pi} \int d\hat{k} \sum_A F_a^A(\hat{k}) F_b^A(\hat{k}) [1 + \delta_{ab}]. \quad (2.23)$$

The factor of $3/8\pi$ before the integral makes the overlap function approach $1/2$ for distinct pulsars separated by a small angle on the sky.

As discussed in FAQ **Q1**, this normalization choice is arbitrary: the physical quantity is $\langle \Delta T_a(t) \Delta T_b(t') \rangle$ on the lhs of (2.19). We are free to rescale the definitions of $\Gamma_{ab}(f)$ and $H(f)$ (given in (2.22) and (2.18)) in any way that we want provided that their product (and hence the physical quantity in (2.19)) is unchanged.

Note that the final expression for Γ_{ab} is independent of frequency. We have factored out a frequency-dependent term that is independent of the specifics of the particular pulsars being correlated. This is a consequence of being able to drop the three exponential terms in (2.21). (See FAQ **Q5** for a related discussion.)

Simple symmetry arguments show that the integral in (2.23) can only depend upon the angle γ_{ab} between the lines of sight to the two pulsars. Without loss of generality, place pulsar a on the z -axis and pulsar b in the xz -plane so that $\hat{p}_a = \hat{z}$ and $\hat{p}_b = \sin \gamma_{ab} \hat{x} + \cos \gamma_{ab} \hat{z}$. The polarisation tensors needed to calculate $F_a^A(\hat{k})$ and $F_b^A(\hat{k})$ are defined by (2.3), with \hat{k} , \hat{l} , \hat{m} given in (2.4). The integral can be approximated numerically or evaluated analytically using contour integration, see e.g., [5–7, and 16]:

$$\Gamma_{ab} \equiv \frac{1}{2} + \frac{3}{2} \left(\frac{1 - \cos \gamma_{ab}}{2} \right) \left[\ln \left(\frac{1 - \cos \gamma_{ab}}{2} \right) - \frac{1}{6} \right] + \frac{1}{2} \delta_{ab}, \quad (2.24)$$

where $\cos \gamma_{ab} = \hat{p}_a \cdot \hat{p}_b$. This is an analytic expression for the Hellings and Downs correlation for pulsar timing, expressed as a function of the angular separation between the directions to a pair of pulsars. A plot of this expected correlation is shown in the left panel of Figure 8, and also as the black dashed curve in Figure 1.

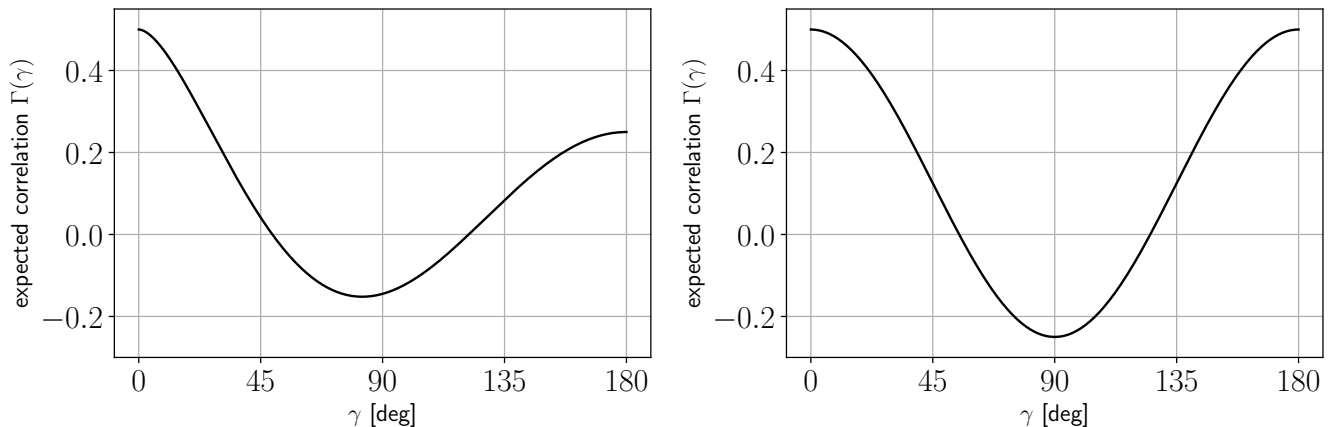


FIG. 8. Left panel: Hellings and Downs correlation for pairs of PTA pulsars. Right panel: The Hellings and Downs correlation for pairs of short-arm LIGO-like detectors. Both have been normalized to 1/2 at zero angular separation. Note that the zero angular separation in the left hand panel corresponds to a pair of pulsars located close on the sky but at significantly different distances. If they are much closer than a GW wavelength, or if they are the same pulsar, then the correlation doubles to unity.

We leave it as an exercise for the reader to show that a similar calculation of the overlap function for an array of “short-arm” LIGO-like detectors yields

$$\Gamma_{ab} = \frac{1}{2} P_2(\cos \gamma_{ab}), \quad (2.25)$$

where $P_2(x)$ is the $l = 2$ Legendre polynomial. For this calculation, you will need to replace the response functions $R^A(f, \hat{k})$ in (2.20) with the short-arm limiting expressions (2.11), and assume that the exponential term involving the detector locations can again be ignored. (But see FAQ **Q5** regarding the calculation of overlap functions for real ground-based interferometers.) This substitution simplifies the integrand in (2.23) to quadratics in $\sin \phi$ and $\cos \phi$ and quartics in $\cos \theta$. The short-arm overlap function is plotted in the right panel of Figure 8. Since the short-arm overlap function only involves the $l = 2$ Legendre polynomial, it is an example of a *purely quadrupolar* overlap function.

Finally, to return to the original question about why the Hellings and Down correlation has different values at 0° and 180° , we plot the integrand $F_1^+(\hat{k})F_2^+(\hat{k}) + F_1^\times(\hat{k})F_2^\times(\hat{k})$ of the Hellings and Downs correlation for these two different cases in the left panel of Figure 9. It is apparent from this plot that if the GWB consisted of waves that only came from directions *perpendicular* to the Earth-pulsar baselines (so in the xy -plane of this plot), then the values of the Hellings and Downs correlation at 0° and 180° would be exactly the same. But since an isotropic GWB has equal contributions from GWs coming from *all* different directions on the sky, the Hellings and Downs correlation for the case $\hat{p}_1 = \hat{p}_2$ will be larger than that for $\hat{p}_1 = -\hat{p}_2$. Why these values differ by exactly a factor of two is the topic of the next question.

Q3: *Is there a simple way to see that the value of the Hellings and Downs correlation for two pulsars separated by 180° is half that for 0° angular separation?*

A3: Yes, but to prove this we need to do a few calculations.

We start with (2.23) for the Hellings and Downs correlation and (2.12) for the Earth-term-only response function. Taking the two pulsars to point in the same direction ($\hat{p}_1 = \hat{p}_2 = \hat{z}$), we have

$$\sum_A F_1^A(\hat{k})F_2^A(\hat{k}) = \frac{1}{4}(1 + \cos \theta)^2. \quad (2.26)$$

Having them point in opposite directions ($\hat{p}_1 = -\hat{p}_2 = \hat{z}$) leads to

$$\sum_A F_1^A(\hat{k})F_2^A(\hat{k}) = \frac{1}{4}(1 + \cos \theta)(1 - \cos \theta) = \frac{1}{4} \sin^2 \theta. \quad (2.27)$$

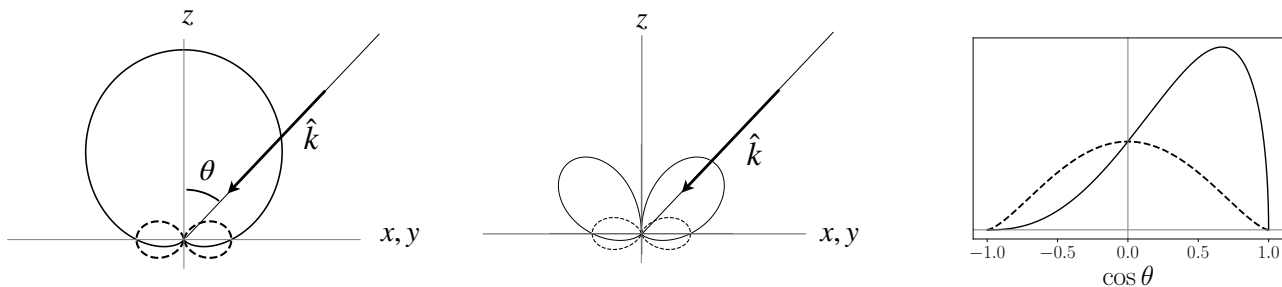


FIG. 9. Integrands of the Hellings and Downs correlation for two pulsars separated by 0° ($\hat{p}_1 = \hat{p}_2 = \hat{z}$, solid curve) and by 180° ($\hat{p}_1 = -\hat{p}_2 = \hat{z}$, dashed curve). The first two panels are polar plots, which are axially symmetric about the z -axis. The left plot shows $F_1^+(\hat{k})F_2^+(\hat{k}) + F_1^\times(\hat{k})F_2^\times(\hat{k})$. The right plot includes an additional factor of $\sin \theta$, which arises when integrating over θ . The right panel is the same as the middle plot, but shown as a function of $\cos \theta$. The area under the solid curve is twice the area under the dashed curve.

These functions are plotted in Figure 9, where θ is the usual polar angle measured with respect to the z -axis. Multiplying by $3/8\pi$ and integrating over the sphere $\int_0^{2\pi} d\phi \int_0^\pi d\theta \sin \theta$ we find

$$\Gamma_{12} = \frac{1}{2} \quad (\text{for } \hat{p}_1 = \hat{p}_2 = \hat{z}), \quad \Gamma_{12} = \frac{1}{4} \quad (\text{for } \hat{p}_1 = -\hat{p}_2 = \hat{z}). \quad (2.28)$$

From the three panel plots in Figure 9, we see that when the two pulsars both point in the \hat{z} direction, the majority of support for the overlap function comes from sky directions $\hat{n} = -\hat{k}$ having $z > 0$. When the two pulsars point in opposite directions, $\hat{p}_1 = -\hat{p}_2 = \hat{z}$, the majority of support for the overlap function comes from sky directions having $z < 0$, which is a smaller contribution.

Visual inspection of the areas under the two curves shown in the rightmost panel of Figure 9 shows why the value of the HD curve for two pulsars separated by 0° is twice as large as that for two pulsars separated by 180° .

Q4: *Why isn't the most-negative value of the Hellings and Downs correlation at 90° ?*

A4: Again, this is because the Earth-term-only response function is not symmetric under $\hat{u} \rightarrow -\hat{u}$. If the Hellings and Downs correlation were purely quadrupolar then its most-negative value would be exactly at 90° , as it is for the case of an array of short-arm LIGO-like detectors (see the right panel of Figure 8). If it had only even multipoles (no odd- l terms) then it would be reflection symmetric about 90° but might not have its minimum there.

Although the dominant contribution to the Hellings and Downs correlation is the quadrupole pattern $P_2(\cos \gamma)$, there are non-zero contributions from all higher order l -modes as well. We leave it as an exercise for the reader to show that

$$\Gamma(\gamma) = \frac{3}{2} \sum_{l=2}^{\infty} (2l+1) c_l P_l(\cos \gamma), \quad \text{where} \quad c_l = \frac{1}{(l+2)(l+1)l(l-1)}. \quad (2.29)$$

To obtain this result, you need to use (a) the orthogonality property

$$\int_{-1}^1 dx P_l(x) P_{l'}(x) = \frac{2}{2l+1} \delta_{ll'} \quad (2.30)$$

of the Legendre polynomials, where $x \equiv \cos \gamma$, (b) Rodrigues' Formula for Legendre polynomials, and (c) integration by parts. See equations (97)–(105) in [17] for a step-by-step derivation of (2.29).

Figure 10 compares approximate versions of the Hellings and Downs correlation, terminating the sum at different maximum values $l_{\max} = 2, 3, 4, 5$. Since the c_l 's in (2.29) fall off like $1/l^4$, only a few values of l are needed to get a very good approximation.

Q5: *Why is the Hellings and Downs correlation frequency independent, whereas overlap functions for ground-based interferometers are frequency dependent?*

A5: Actually, the Hellings and Downs correlation for timing residual measurements *is* frequency dependent. But this $1/(2\pi f)^2$ frequency dependence is the same for *all* pairs of pulsars and hence can be “factored out” of the Hellings and Downs correlation function (2.22) and absorbed into the strain spectrum $H(f)$ in (2.19). (This changes

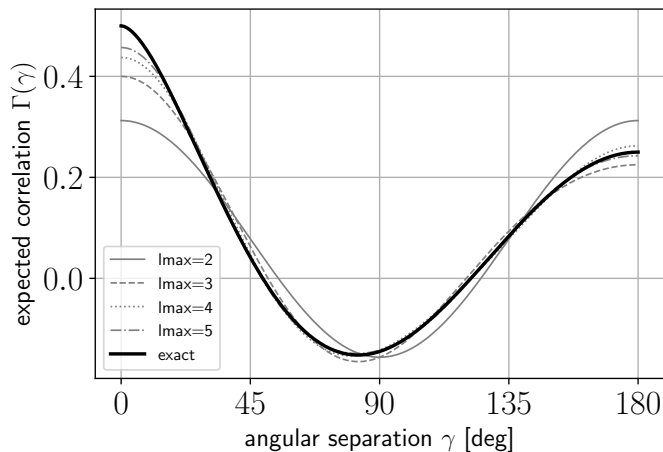


FIG. 10. Approximations to the Hellings and Downs curve (solid black) obtained by terminating the sum in (2.29) with two to five Legendre polynomials (grey curves).

the dimensions of $H(f)$ from $\text{strain}^2 \text{Hz}^{-1}$ to $\text{s}^2 \text{Hz}^{-1}$.) This factorization is possible because the exponential terms in (2.21) that depend on the distances to the pairs of pulsars defining the correlation and the locations of the radio telescopes making the measurements can be ignored when calculating the expected correlation, for the reasons discussed in the sentences following (2.21).

For ground-based interferometers, the frequency dependence of the correlation comes from the exponential factor $e^{-i2\pi f \vec{k} \cdot (\vec{r}_a - \vec{r}_b)/c}$ in (2.20), since $R^A(f, k)$ is independent of frequency in the short-arm limit, see (2.11). Here, \vec{r}_a and \vec{r}_b denote the position vectors of the two interferometers's central stations. For two such detectors on Earth, the distance $D_{ab} \equiv |\vec{r}_a - \vec{r}_b|$ between the stations is comparable to the wavelength $\lambda \equiv c/f$ (hundreds to thousands of km) of the GWs that these detectors are sensitive to. Hence, it cannot be ignored as we were able to do for the long-arm PTA pulsar calculation in (2.21). So even though the individual ground-based interferometers operate in the short-arm limit $L \ll \lambda$, it is *not* also the case that $D_{ab} \ll \lambda$, but rather $\lambda \lesssim D_{ab}$. Since the frequency dependence for ground-based interferometers is tied to the detector locations, it cannot be factored out of the correlation $\Gamma_{ab}(f)$ and absorbed into $H(f)$.

Q6: *Is the Hellings and Downs correlation only relevant for isotropic GWBs?*

A6: No. The Hellings and Downs pattern is a robust prediction for the correlation produced by any (small or large) set of non-interfering GW sources, provided that many pairs of pulsars, uniformly distributed on the sky, are employed. This was first demonstrated for the special case of GWs produced by a single black hole binary in [18]. It was then extended to an arbitrary set of non-interfering sources in [6], which further exploited pulsar averaging. Note that for interfering sources, we do *not* expect to recover exactly the HD pattern (see FAQ **Q7** and [6]).

The original (and traditional) approach to obtain the Hellings and Down correlation is to consider just one pair of pulsars, and to average their correlation over GW propagation directions, assuming that the sources are unpolarized and isotropic on the sky [5]. In references [18] and [6], somewhat involved calculations were done to show the equivalence of the two approaches.

But, in fact, one can show the equivalence with no calculation. The geometry of the pulsar averaging is equivalent to that of the isotropic GW-source averaging after a series of Euler-angle rotations, provided for the GW averaging calculation one averages over the polarization angle ψ *in addition* to the GW propagation direction $\hat{k} = \hat{k}(\theta, \phi)$. Note that the original [5] calculation obscures this point by not giving enough detail. To reproduce the result, one must also assign a polarization to each source, and average over that. Hence, averages must be calculated with respect to three angles, not just two.

To see the equivalence purely from geometry, start with the GW averaging calculation. As often done, without loss of generality, put \hat{p}_1 along the z -axis and \hat{p}_2 in the xz -plane, so that $\hat{p}_2 = \sin \gamma \hat{x} + \cos \gamma \hat{z}$. Pulsar averaging is carried out with respect to the angular coordinates of \hat{p}_1 (polar coordinate θ , azimuthal coordinate ψ) and those of \hat{p}_2 (which lies on a cone about \hat{p}_1 with fixed half-opening angle γ , with its location on the cone parametrized by $\phi \in [0, 2\pi)$). See Figure 11 and compare with Figure 5 of [6].

The sequence of rotations that is needed to go from GW-source averaging to pulsar averaging is to first rotate by $-\phi$ about the z axis, which moves the GW propagation direction \hat{k} into the xz -plane and \hat{p}_2 around a cone with

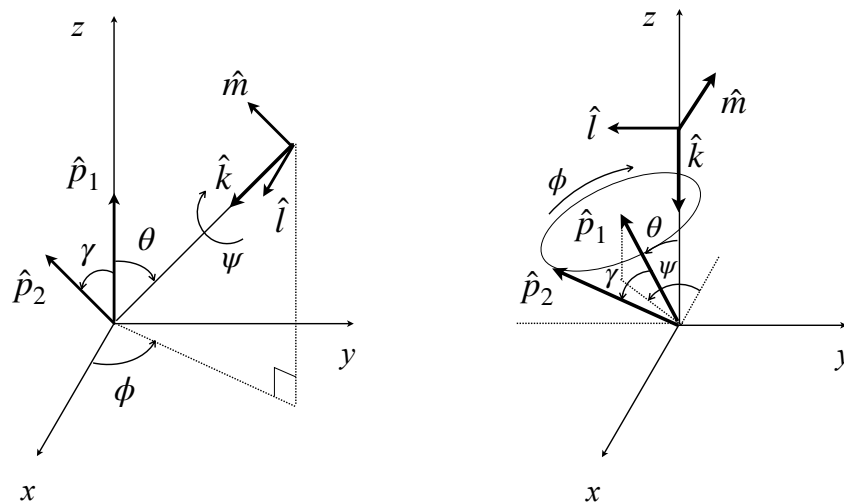


FIG. 11. Isotropic GW-source averaging (left panel) and pulsar averaging (right panel) are equivalent, as can be seen by carrying out a series of rotations.

central axis \hat{p}_1 through angle ϕ . One then rotates by $-\theta$ around the y axis, which puts \hat{k} along $-\hat{z}$, and makes \hat{p}_1 have polar angle θ . Finally, one rotates around \hat{k} (which now points in the $-\hat{z}$ direction) by $-\psi$, which becomes the azimuthal angle for \hat{p}_1 (with respect to the $-x$ axis).

The fact that one obtains the Hellings and Downs correlation from pulsar averaging means that the Hellings and Downs correlation is not restricted to isotropic GWBs. But to exactly recover Hellings and Downs, one must assume that there are no interference cross-terms that enter the correlation (see the discussion following Eq. 4.4 of [6] and the discussion in [19]).

In practice, we do not have an infinite number of pulsar pairs separated by the angle γ . So, to do pulsar averaging, one divides the $N_{\text{pul}}(N_{\text{pul}} - 1)/2$ inter-pulsar correlations into a smaller number N_{bins} of angular separation bins. This form of pulsar averaging is always used to recover the Hellings and Downs curve. For example, for the NANOGrav 15-year analysis shown in Figure 1, $N_{\text{pul}} = 67$ and $N_{\text{bins}} = 15$, which implies that the estimated correlation value in each angular separation bin involved an average of approximately 150 pulsar pairs.

Q7: *In the future, PTA observations will be carried out with many more pulsars. We also expect that the GWB signal contribution will grow much faster than pulsar noise as the observation time increases. Does that mean that at some time in the distant future, we'll exactly recover the Hellings and Downs correlation?*

A7: This would be the case if the GWB were produced by a set of discrete non-interfering sources. (See for example Section IV and Equation 4.1 of [6] and the discussion in [19].)

But it is much more likely that our Universe contains many GW sources radiating at frequencies that are close enough together that they cannot be resolved individually over the time-span of the PTA experiments (say, tens to hundreds of years). This means that the GWB is produced by a sum of *interfering sources*. An example of such a GWB is the “confusion noise” created by a uniform distribution of sources emitting monochromatic GWs with random phases, but occupying *the same frequency bin*. In this case, pulsar-averaged noise-free measurements over an infinite number of pulsars pairs with the same angular separation do not give exactly the Hellings and Downs curve.

If we have an infinite collection of universes, each of which has different random phases, and we were also able to average over all of those universes, then we would get exactly the Hellings and Downs curve. But in any given universe, we would find something different from the Hellings and Downs curve. The (mean squared) difference between what would be observed in any given universe, and the average over many universes, is called the “cosmic variance”.

To compute this cosmic variance $\sigma_{\text{cosmic}}^2(\gamma)$ for a given ensemble of model universes, we express the pulsar-averaged correlation Γ_i in the i th universe as a deviation $\Delta\Gamma_i$ away from the many-universe average Γ :

$$\Gamma_i(\gamma) = \Gamma(\gamma) + \Delta\Gamma_i(\gamma) \quad (\text{for universe } i). \quad (2.31)$$

Then

$$\langle \Gamma_i(\gamma) \rangle = \Gamma(\gamma) \quad \text{but} \quad \langle (\Gamma_i(\gamma) - \Gamma(\gamma))^2 \rangle = \langle \Delta\Gamma_i^2(\gamma) \rangle \equiv \sigma_{\text{cosmic}}^2(\gamma), \quad (2.32)$$

where the ensemble-average angle brackets denote an average over i . See [6, 19, and 20] for explicit calculations of $\sigma_{\text{cosmic}}^2(\gamma)$ for several simple but realistic models of the Universe.

Q8: *Assuming noise-free observations, are the fluctuations away from the expected Hellings and Downs curve due solely to the pulsar-term contributions to the timing residual response?*

A8: No. While the pulsar terms do contribute to deviations away from the expected Hellings and Downs correlation, there are other more fundamental sources of such deviations. (i) Timing residual measurements from two different pulsar pairs separated by the same angle γ but pointing in different directions on the sky will have different correlations due to the different parts of the GWB that they are sensitive to. So if the pulsar pairs are not uniformly distributed, this gives deviations. (ii) For interfering sources, even with infinite pulsar averaging as described in FAQ **Q7**, there will be fluctuations away from expected Hellings and Downs correlation that come from the Earth-term-only response functions.

For a given pulsar pair, the pulsar-term contributions to the timing residual response *add* to the fluctuations, with the same root-mean-square amplitude as the Earth terms. But, as mentioned in the previous paragraph, they are not the sole source of the fluctuations away from the Hellings and Downs correlation, and as more and more pairs of pulsars are averaged together at a particular angular separation, this pulsar-term contribution becomes insignificant.

Q9: *Why does the Hellings and Downs recovery plot shown in Figure 1) (from the recent NANOGrav publication [4]) have error bars that are much larger than one would expect for the reported 3 to 4 σ detection significance?*

A9: While the match at any given angle is not very close, the detection significance comes from comparing two “waveforms” to compute a single “signal-to-noise ratio”, in the same way that LIGO compares snippets of its noisy time-domain data to noise-free chirp templates. Effectively, this signal-to-noise ratio sums products of the observed pulsar-pair correlations with the “expected waveform” given by the Hellings and Downs curve. The individual terms of this sum are inversely weighted by estimates of their expected squared values *in the absence* of the Hellings and Downs correlations. So, even though the match at any given angle is not very close, the overall agreement is actually quite good. In fact, NANOGrav obtains significance estimates from two types of analyses:

(i) A 3.8σ significance determined using frequentist *detection statistics*, such as the noise-weighted inner product of the observed correlations with the expected Hellings and Downs correlation, as described above. This is the “stochastic equivalent” of the deterministic *matched filter statistic* used by LIGO to search for individual compact binary coalescence “chirp” signals. The distribution that would be expected in the absence of a GWB is estimated by artificially introducing phase shifts which remove the Hellings and Downs correlations (see the right panel of Figure 3 in Ref. [4]). The observed value of the detection statistic lies in the “tail” of the null distribution, and thus corresponds to high detection significance.

(ii) A 3.0σ significance obtained via a Bayesian analysis. This analysis compares the evidence for a data model containing the Hellings and Downs spatial correlations to a model without these correlations. The ratio of the evidences is 226, which is the “betting odds” for which of the two models is correct. The significance of the value 226 is then estimated from the null distribution of the evidence ratio, again constructed using phase shifts (see both Figure 2 and the left panel of Figure 3 in Ref. [4]).

What is shown in Figure 1 for the NANOGrav 15-year analysis [4] is instead a “self-consistency check” of the pulsar-pair cross-correlations, *calculated under the hypothesis that a GWB with Hellings and Downs correlations is present in the data*, with an overall amplitude estimated from auto-correlation measurements, and assuming that there are no unknown sources of noise with similar spatial correlations. The estimated correlations and error bars are optimally weighted combinations of approximately 150 correlation measurements in each angular separation bin, which include the covariances between the correlations induced by the GWB. If the observed data are consistent with the Hellings and Downs correlation model then these point estimates and 1σ error bars will cross the expected Hellings and Downs curve approximately 70% of the time on average. See [20] for more details.

III. CONCLUSION

We have answered a number of frequently asked questions (FAQs) about the Hellings and Downs correlation for PTA searches. Many of these questions arise from inadvertently applying intuition about the effects of GWs on a detector, which are appropriate for LIGO-Virgo observations, to the case of PTA observations, where some of that intuition is no longer valid. The key difference is that a PTA detector has “arm lengths” (Earth-pulsar distances) much longer than the wavelengths of the GWs that they are sensitive to, while ground-based laser interferometers (like LIGO, Virgo, KAGRA) operate in the opposite (i.e., “short-arm”) limit.

By calculating the response of a one-arm, one-way detector to a passing GW, and then comparing the limiting expressions of this response for “short-arm” LIGO-like detectors and “long-arm” PTA pulsar detectors, we were able

to obtain qualitative and quantitative answers to these questions. We hope that this “Hellings-and-Downs correlation FAQ sheet” will help to inform the scientific community and educate the general public about the current and ongoing PTA searches for GWs.

ACKNOWLEDGMENTS

This paper and its “FAQ sheet” format arose from discussions that JDR had with his wife and with several students attending the “MaNiTou Summer School on GWs,” held from 3 July to 8 July 2023, in Nice, France. JDR acknowledges past conversations with numerous NANOGrav colleagues about various aspects of these topics, and financial support from the NSF Physics Frontier Center Award PFC-2020265. He also thanks colleagues Nelson Christensen and Marie-Anne Bizouard for their support and hospitality while visiting the Artemis Lab, Observatoire Cote D’Azur in June and July 2023, where the majority of this paper was written.

-
- [1] Daniel J. Reardon, Andrew Zic, Ryan M. Shannon, *et al.*, “Search for an Isotropic Gravitational-wave Background with the Parkes Pulsar Timing Array,” *ApJ* **951**, L6 (2023).
 - [2] Heng Xu, Siyuan Chen, Yanjun Guo, *et al.*, “Searching for the Nano-Hertz Stochastic Gravitational Wave Background with the Chinese Pulsar Timing Array Data Release I,” *Research in Astronomy and Astrophysics* **23**, 075024 (2023).
 - [3] J. Antoniadis, P. Arumugam, S. Arumugam, *et al.*, “The second data release from the European Pulsar Timing Array III. Search for gravitational wave signals,” *arXiv e-prints*, arXiv:2306.16214 (2023).
 - [4] Gabriella Agazie, Akash Anumalapudi, Anne M. Archibald, *et al.*, “The NANOGrav 15 yr Data Set: Evidence for a Gravitational-wave Background,” *ApJ* **951**, L8 (2023).
 - [5] Ronald W. Hellings, “Pulsar timing and gravitational waves,” in *Relativistic Gravitational Experiments in Space: proceedings of NASA Workshop, Annapolis, Maryland, June 28-30, 1988*, NASA Conference Publication, Vol. 3046 (1989) pp. 93–97.
 - [6] B. Allen, “Variance of the Hellings-Downs correlation,” *Phys. Rev. D* **107**, 043018 (2023).
 - [7] Melissa Anholm, Stefan Ballmer, Jolien D. E. Creighton, Larry R. Price, and Xavier Siemens, “Optimal strategies for gravitational wave stochastic background searches in pulsar timing data,” *Phys. Rev. D* **79**, 084030 (2009).
 - [8] C. W. Misner, K. S. Thorne, and J. A. Wheeler, *Gravitation*, Misner:1973 (W.H. Freeman and Company, San Francisco, 1973).
 - [9] James B. Hartle, *Gravity: An Introduction to Einstein’s General Relativity* (Addison Wesley, 2002).
 - [10] Joseph D. Romano, “Searches for stochastic gravitational-wave backgrounds,” *arXiv e-prints*, arXiv:1909.00269 (2019).
 - [11] S. Detweiler, “Pulsar timing measurements and the search for gravitational waves,” *ApJ* **234**, 1100–1104 (1979).
 - [12] L. Isserlis, “On a formula for the product-moment coefficient of any order of a normal frequency distribution in any number of variables,” *Biometrika* **12**, 134–139 (1918), note that Isserlis’ theorem is often called “Wick’s theorem” in the physics community, although the Wick’s work was three decades later.
 - [13] Éanna É. Flanagan, “Sensitivity of the Laser Interferometer Gravitational Wave Observatory to a stochastic background, and its dependence on the detector orientations,” *Phys. Rev. D* **48**, 2389 (1993).
 - [14] N. Christensen, “Optimal detection strategies for measuring the stochastic gravitational radiation background with laser interferometric antennas,” *Phys. Rev. D* **55**, 448–454 (1997).
 - [15] Lee Samuel Finn, Shane L. Larson, and Joseph D. Romano, “Detecting a stochastic gravitational-wave background: The overlap reduction function,” *Phys. Rev. D* **79**, 062003 (2009).
 - [16] Fredrick A. Jenet and Joseph D. Romano, “Understanding the gravitational-wave Hellings and Downs curve for pulsar timing arrays in terms of sound and electromagnetic waves,” *American Journal of Physics* **83**, 635–645 (2015).
 - [17] Jonathan Gair, Joseph D. Romano, Stephen Taylor, and Chiara M. F. Mingarelli, “Mapping gravitational-wave backgrounds using methods from CMB analysis: Application to pulsar timing arrays,” *Phys. Rev. D* **90**, 082001 (2014).
 - [18] Neil J Cornish and A Sesana, “Pulsar timing array analysis for black hole backgrounds,” *Classical and Quantum Gravity* **30**, 224005 (2013).
 - [19] Bruce Allen, “Will pulsar timing arrays observe the Hellings and Downs correlation curve?” in *18th Vulcano Workshop: Frontier Objects in Astrophysics and Particle Physics*, Vol. 74, edited by Antonella Antonelli, Roberto Fusco Femiano, Aldo Morselli, and Gian Carlo Trincherò (2022) pp. 65–80.
 - [20] Bruce Allen and Joseph D. Romano, “The Hellings and Downs correlation of an arbitrary set of pulsars,” (2023).